IEEE Access
Multidisciplinary ⋮ Rapid Review ⋮ Open Access Journal

Received August 27, 2021, accepted September 15, 2021, date of publication September 17, 2021,
date of current version September 24, 2021.

Digital Object Identifier 10.1109/ACCESS.2021.3113765

Magnetic Force-Propelled 3D Locomotion Control for Magnetic Microrobots via Simple Modified Three-Axis Helmholtz Coil System

ARMANDO RAMOS-SEBASTIAN[1,2], (Graduate Student Member, IEEE), AND SUNG HOON KIM[1,3], (Member, IEEE)

[1]Department of Electronic Convergence Engineering, Wonkwang University, Iksan 54538, Republic of Korea
[2]Department of IT Convergence Mechatronics Engineering, Jeonbuk National University, Jeonju 54896, Republic of Korea
[3]Wonkwang Institute of Material Science and Technology, Wonkwang University, Iksan 54538, Republic of Korea

Corresponding author: Sung Hoon Kim (kshoon@wku.ac.kr)

This work was supported in part by Korea Medical Device Development Fund grant funded by the Korean Government (the Ministry of Science and ICT, the Ministry of Trade, Industry and Energy, the Ministry of Health and Welfare, and the Ministry of Food and Drug Safety) under Project KMDF_PR_20200901_0130 and Project 9991006803, in part by the Basic Science Research Program of the Ministry of Science and ICT under Grant 2020R1A4A3079595, and in part by the National Research Foundation of Korea (NRF) grant funded by the Korean Government (the Ministry of Science and ICT) under Grant 2018R1C1B6003491.

ABSTRACT Magnetic microrobots are propelled by magnetic fields or magnetic field gradients generated by electromagnetic systems. Generally, 3D Helmholtz coils systems are used for microrobot propulsion, because of their low power consumption, ease of manufacture, and ease of control, for which, only three power supplies are required. Systems of this kind can only generate uniform magnetic fields, which limits their range of applications. However, generating both uniform magnetic fields and gradients typically requires more coils and power supplies, resulting in large expensive energy-intensive systems with complicated control algorithms. Although the aforementioned systems can control magnetic robots with up to 6 degrees of freedom (DOFs), most existing applications at the micro/nanoscale only require 2 rotational DOFs and 1 translational DOF. Here, we propose a new control system capable of producing 3D uniform magnetic fields with 3 DOFs and 3D gradients with 1 DOF. With this system, one pair of coils in a traditional 3D Helmholtz coil system is modified, to enable independent control of the individual coils directing a selected axis, while the configuration of the remaining two pairs of coils is unchanged. This results in a control system with low power consumption, and a simple control algorithm that can be easily applied to existing 3D Helmholtz systems, as it only requires the addition of a power supply. In combination with the developed system, we also propose a new control algorithm applicable to both permanently and temporarily magnetized microrobots, and verify this experimentally.

INDEX TERMS Electromagnetic actuation system, magnetic force control, magnetic gradient, magnetic microrobots.

I. INTRODUCTION

The locomotion of magnetic microrobots is achieved through control of magnetic forces and torques generated by systems composed of magnets or electromagnets [1], [2]. Three pairs of electromagnetic coils are typically used in a Helmholtz coil configuration [3], [4] for the generation of uniform magnetic fields (UMFs); however, the use of saddles coils is common too [5], [6]. As the electric current flowing in individual coils in each pair of UMF-generating coils is the same, in most cases, both coils are connected in series and controlled with a single power supply, resulting in a system with three pairs of coils and three power supplies. Though control of this kind of system is the simplest, as they are unable to generate magnetic forces, their applications are typically limited to microrobots with 2 rotational degrees of freedom (DOFs), such as helical microrobots [7], [8] and microrobots with flexible tails [9], [10]. Though UMFs alone can be used for some biomedical applications like unclogging blood vessels [11], [12], it has been proved that a gradient magnetic

The associate editor coordinating the review of this manuscript and approving it for publication was Wenxin Liu.

field (GMF) can enhance the drilling performance of microrobots, and provide them with new functions [13]–[15].

It is thus desirable for electromagnetic systems to also be able to produce 3D magnetic forces with at least 1 DOF.

To generate GMFs, researchers typically add pairs of Maxwell coils, which have the advantage of producing a uniform gradient magnetic field, to the basic Helmholtz system. Consequently, the control algorithm for this system remains simple. When such systems were first introduced, researchers tended to use one pair of Maxwell coils per axis [16], [17], with the number of pairs of Maxwell coils decreasing as development continued [18]. It was eventually demonstrated that the application of a 3D force to a microrobot with a single pair of Maxwell coils and a 3D Helmholtz system is feasible [19]. However, though the control algorithm for this kind of system is simple, their power consumption and size increase with the number of coils, while the working space remains small. Recently, a system [20] using this coil configuration was used to control the motion of a cylindrical microrobot, by controlling the directional gradient independently of the UMF direction [21], for a maximum of 6 DOFs. However, as the system requires the use of 12 coils, it has a small working space and consumes more power than a standard 3D Helmholtz coil system.

A different approach for producing UMFs and GMFs simultaneously is to control every coil in the 3D Helmholtz coil system independently [22]–[26]. Control of the motion of a cylindrical magnetic microrobot by such a system was recently demonstrated, with a maximum position error of up to 0.25× the length of the microrobot reported [27]. Although in these systems the total number of coils remains as six, the number of power supplies required increases to six, while the control system also becomes more complicated, increasing the overall cost of the system.

A large variety of electromagnetic systems exist as well those based on the Helmholtz coil configuration, achieving up to 6 DOFs for magnetic microrobots. However, in such systems, the number of coils exceed the number used in the Helmholtz configuration, and the working space is smaller. In addition, because they do not produce uniform magnetic fields or uniform magnetic field gradients, they also require more complicated and expensive control systems [28]–[30].

Thus far, most developed biomedical applications for magnetic microrobots can be executed by microrobots with 2 rotational DOFs and 1 translational DOF, especially when using untethered magnetic microrobots because they are free to rotate. When using a magnetic force to induce locomotion, the direction of locomotion usually coincides with the magnetization direction. These applications include the active guidance of magnetic catheters, stent delivery, and unclogging motions [31], [32]; driving of endoscopic capsules for imaging, biopsy, and drug delivery [33], [34]; and locomotion and targeted drug delivery using soft magnetic microrobots [35]–[37].

In this study, we propose a modification to the traditional 3D Helmholtz coil system, to reduce the number of coils and power supplies, required to produce a 3-DOF UMF and a 1-DOF GMF simultaneously, while maintaining the simplicity of the control algorithm. The modification consists of arbitrarily splitting the series connection of one of the three pairs of coils, and including an additional power supply. This modification can be easily applied to any existing 3D Helmholtz coil system, eliminating the need to invest in the development of an additional system, or to include extra coils. Furthermore, since the only investment required is an additional power supply, this modification is the cheapest way of implementing GMFs. We also propose a simple but precise control algorithm for magnetic force-based 3D locomotion using the proposed system, which is capable of controlling both permanent magnet microrobots and temporarily magnetized microrobots.

II. MODIFIED HELMHOLTZ SYSTEM AND CONTROL METHOD

A. ELECTROMAGNETIC SYSTEM CONFIGURATION

The proposed control system is based on a traditional 3D Helmholtz coil configuration composed of three pairs of coils, with each coil in a pair connected in series, and each pair of coils controlled by one power supply, as depicted in Fig. 1(a). In the modified system, two pairs of coils (H_x, H_y) are maintained in their original configuration (each coil in a pair is connected in series, and each pair of coils is controlled with a single power supply). However, the remaining coils (constituting the H_z pair in this case) are connected to different power supplies each, and controlled independently, resulting in a system composed of six coils and four power supplies. As in a traditional Helmholtz system, when the same current flows through H_{z1} and H_{z2}, a UMF is created. In combination with the UMFs created by the other two pairs of coils, the system creates a 3D UMF with 3 DOFs, as shown in Fig. 1(b). In contrast, when currents with the same magnitude flow in opposite directions through H_{z1} and H_{z2}, a non-uniform magnetic field is created. As shown in Fig. 1(c), the magnetic field varies along the three vectorial directions; hence, a 3D magnetic gradient with 1 DOF is produced.

To probe the ability of the system to generate a 3D magnetic force, we evaluated the locomotion of a magnetic microrobot using this magnetic force to drive the microrobot in a 3D space. The microrobot used was a spherical magnet, and it possessed a total of 3 DOFs: 2 rotational DOFs perpendicular to the magnetic moment of the magnet and 1 translational DOF, whose axis was the mirrored axis of the microrobot's magnetic moment axis (in the absence of other forces) with respect to the H_z coils' axis, as shown in Fig. 2(a).

To control the microrobot, we used the UMF to exert a torque on the robot; this caused its magnetic moment to align with the direction of the magnetic field, as shown in Fig. 2(b). Furthermore, as depicted in Fig. 2(c), when currents with the same magnitudes but opposite directions flow through the pair of coils H_z, the magnitude of the magnetic field is small. Hence, it has a negligible effect on the orientation of the robot. However, because a magnetic gradient still exists, a force

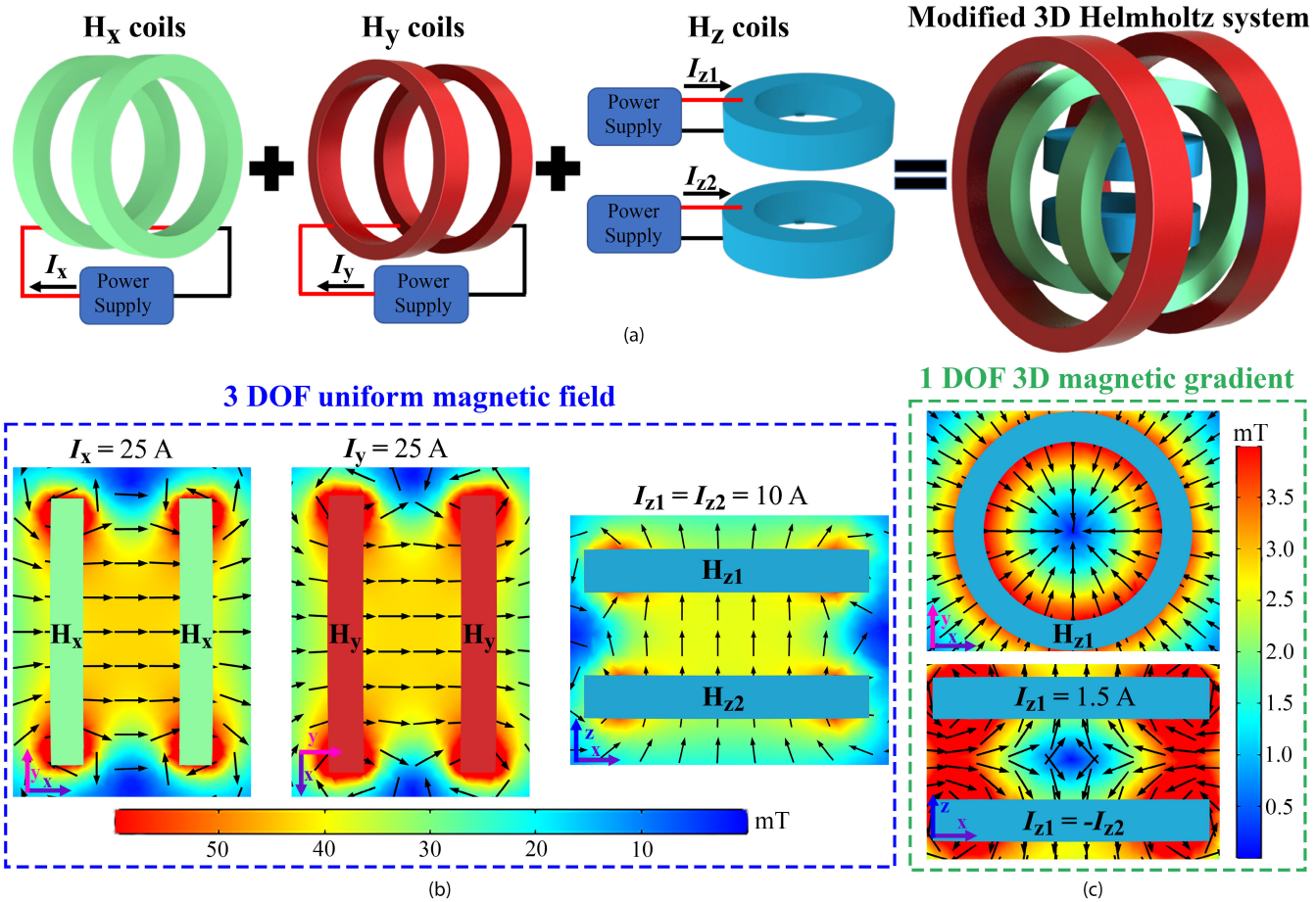

FIGURE 1. (a) Configuration of modified 3D Helmholtz coil system, comprising two pairs of coils (H_x, H_y) each controlled with a single power supply, and a pair of coils (H_z) in which each coil is controlled individually. (b) Magnetic field distribution for each pair of Helmholtz coils producing a 3-DOF uniform magnetic field. (c) Magnetic field distribution when currents with the same magnitudes but opposite directions flow in the pair of coils H_z, producing a magnetic gradient that generates a 3D force with 1 DOF.

is exerted on the microrobot; this pushes it along an axis that is mirrored with its magnetization direction, as shown in Fig. 2(c). Hence, the orientation and direction of motion of a magnetic microrobot can be controlled by superpositioning UMFs on a non-uniform magnetic field.

B. FORCE ANALYSIS OF A MAGNETIC MICROROBOT

In this section, we derive the UMFs produced by the electromagnetic system by modelling the coils controlling the z axis as a Helmholtz pair, H_z, and the GMFs, by considering them as a gradient pair with the same specifications, G_z, in a separate analysis. These derivations were conducted to simplify design of the control procedures for the electromagnetic system. The magnetic flux density produced by the three pairs of circular Helmholtz coils H_x, H_y, H_z and is:

$$\mathbf{B} = \begin{bmatrix} B_x \\ B_y \\ B_z \end{bmatrix} = \left(\frac{4}{5}\right)^{3/2} \mu_0 \begin{bmatrix} n_x I_x / R_x \\ n_y I_y / R_y \\ n_z I_z / R_z \end{bmatrix} \tag{1}$$

where n, I, and R are the respective number of turns, electric current, and radius of each pair of coils, μ_0 is the vacuum permeability, and the subindices x, y, and z correspond to the H_x, H_y and H_z pairs of coils, respectively. Except for the electric currents, all the terms in this equation are constants. Hence, the magnetic field can be simplified as:

$$\mathbf{B} = \begin{bmatrix} k_x I_x & k_y I_y & k_z I_z \end{bmatrix}^{\mathrm{T}} \tag{2}$$

where k_x, k_y, and k_z are constants.

Fig. 3 shows the forces that act on the microrobot as it moves through a fluid. The microrobot experiences a gravitational force $\mathbf{F}_g = m_r g_c$ (m_r is the mass of the robot, and g_c is acceleration due to gravity; 9.8 m/s^2), a buoyancy force $\mathbf{F}_b = V_r \rho_f g_c$ (V_r and ρ_f are the volume of the robot and the density of the fluid, respectively) that pushes the magnet to the surface of the liquid, and a drag force $\mathbf{F}_d = 6\pi \mu_f r_m v_f$ (μ_f, v_f, and r_m are the kinematic viscosity of the fluid, and the velocity and radius of the magnetic microrobot, respectively) that opposes the movement of the microrobot in the fluid.

In this study, we define $\mathbf{F}_c$ and $\mathbf{F}_l$ as the gravity compensation and magnetic locomotive forces produced by the coil system. The magnetic force exerted on a microrobot by the

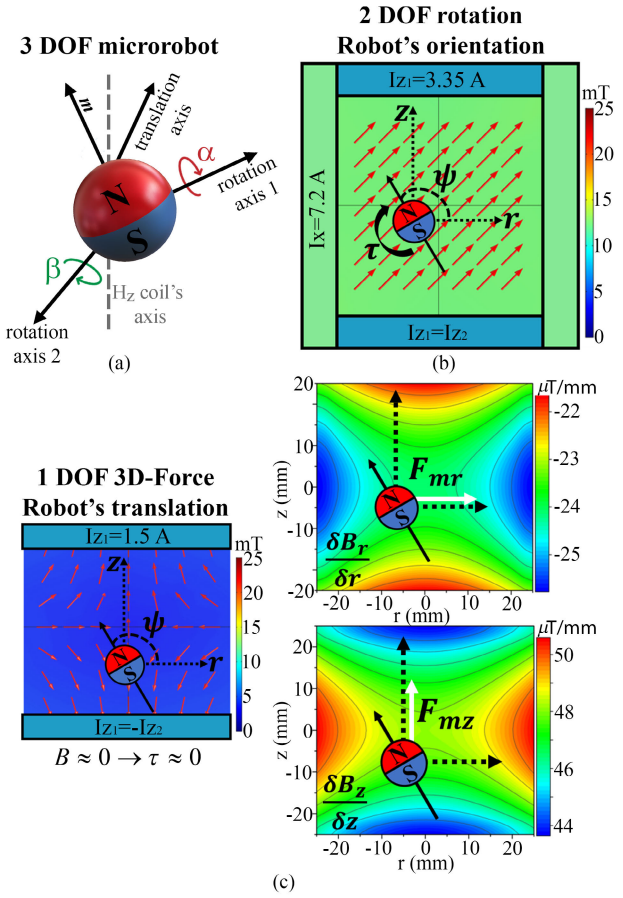

FIGURE 2. (a) Magnetic microrobot with 3 DOFs, i.e., 2 rotational DOFs and 1 translational DOF. (b) UMF produced by the EMA system induces rotation in the magnet, controlling the magnetic moment (*m*) orientation. (c) GMF produced by the EMA system exerts a magnetic force that pushes the microrobot along the mirrored axis of its magnetic moment axis, with respect to the axis of the H_z coils.

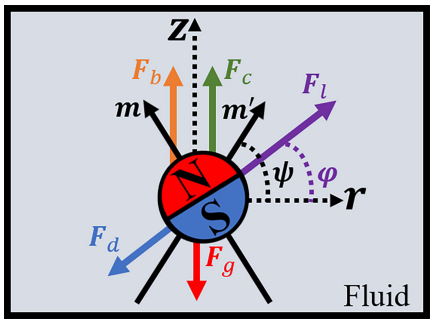

FIGURE 3. Forces acting on a microrobot during motion.

pair of gradient coils is:

$$\mathbf{F}_m = (\mathbf{m} \cdot \nabla)\,\mathbf{B} \tag{3}$$

where $\mathbf{m} = [\mathbf{m}_x\ \mathbf{m}_y\ \mathbf{m}_z]$ is the magnetic moment of the microrobot. Because of the geometry of the gradient coils, the magnitude of the magnetic force in the XY plane varies with the distance from the axis of the coils, and the direction of the axis of the coils, rather than the x or y coordinate. Hence, we analyze the magnetic force in the ZR plane, where z is the vertical axis and r is any axis perpendicular to z. Redefining the magnetic moment of the robot from (3) as $\mathbf{m} = [\mathbf{m}_r\ \mathbf{m}_z]$ thus results in the following:

$$\mathbf{F}_m = \begin{bmatrix} \mathbf{m}_r \dfrac{\delta \mathbf{B}_r}{\delta r} + \mathbf{m}_z \dfrac{\delta \mathbf{B}_r}{\delta z} \\ \mathbf{m}_r \dfrac{\delta \mathbf{B}_z}{\delta r} + \mathbf{m}_z \dfrac{\delta \mathbf{B}_z}{\delta z} \end{bmatrix} \tag{4}$$

Unlike a Maxwell coil pair, with our pair of gradient coils, all four elements in (4) contribute to the total force exerted on the microrobot. Since there are no electric currents in the working space, $\nabla \times \mathbf{B} = 0$ and $\delta \mathbf{B}_r/\delta z = \delta \mathbf{B}_z/\delta r$. Because the magnitude of $\delta \mathbf{B}_z/\delta r$ is much smaller than $\delta \mathbf{B}_z/\delta z$ and $\delta \mathbf{B}_r/\delta r$, its contribution to the overall magnetic force can be neglected, resulting in:

$$\mathbf{F}_m = \begin{bmatrix} \mathbf{m}_r \dfrac{\delta \mathbf{B}_r}{\delta r} & \mathbf{m}_z \dfrac{\delta \mathbf{B}_z}{\delta z} \end{bmatrix}^T \tag{5}$$

As shown in Fig. 2(c), the magnitude of the magnetic gradient varies less than 7% in our working space (50 mm x 50 mm); hence, to simplify the control algorithm and apply it to open-loop control systems, we consider the gradient in the working space to be constant, equaling

$$\mathbf{G} = \begin{bmatrix} -g_z/2 & g_z \end{bmatrix}^T \tag{6}$$

where g_z is the gradient of $\mathbf{B}_z$ in the z-direction, produced by the gradient coils at the center of their axis, and is equal to

$$g_z = k_g I_g \tag{7}$$

where I_g is the electric current flowing in the gradient coils and k_g is a constant that depends on the parameters of the coils. Hence, (5) can be rewritten as:

$$\mathbf{F}_m = \begin{bmatrix} -\mathbf{m}_r g_z/2 & \mathbf{m}_z g_z \end{bmatrix}^T \tag{8}$$

At equilibrium, the vertical forces are balanced, and $\mathbf{F}_z = \mathbf{F}_c + \mathbf{F}_b - \mathbf{F}_g = 0$. This equation can be solved to find the value of g_z required to keep the microrobot floating, giving:

$$g_0 = (\mathbf{F}_g - \mathbf{F}_b)/\mathbf{m}_z \tag{9}$$

To drive the microrobot we include an additional magnetic force for the propulsion of the robot, given by,

$$\mathbf{F}_l = \mathbf{m} \cdot \mathbf{G}_l \tag{10}$$

where $\mathbf{G}_l = \begin{bmatrix} g_{lr} & g_{lz} \end{bmatrix}^T$. Hence, the total magnetic gradient that has to be produced by the coil is:

$$\mathbf{G}_m = \begin{bmatrix} g_{lr} & g_0 + g_{lz} \end{bmatrix}^T \tag{11}$$

Because a vertical force needs to be exerted on the microrobot to compensate the gravity force, the orientation (ψ) of the mirrored axis (***m'***) of the magnetic moment (***m***) and magnetic force do not match its direction of motion (φ). Since a permanent neodymium magnet robot was used in the 3D experiments, we consider the microrobot to align with the direction of the magnetic field upon its application. Hence,

TABLE 1. Specifications of the pairs of Helmholtz coils.

Coils	Number of Turns	Radius	Maximum Magnetic Flux Density	Maximum Magnetic Gradient
H_X	583	14 mm	37.4 mT	320 μT/mm
H_Y	430	22 mm	44 mT	240 μT/mm
H_Z	602	30 mm	45 mT	180 μT/mm

the magnetic moment and the magnetic field direction are the same. Additionally, when they are used, the UMF magnetizes non-permanent magnet microrobots in the direction parallel to the magnetic field. Knowing that $g_{lz} = G_l \sin\varphi$, $g_{lr} = G_l \cos\varphi$, and $G_l = \sqrt{g_{lz}^2 + g_{lr}^2}$, we defined the following system of equations using (11) and (6):

$$\begin{aligned} g_z \sin\psi &= g_0 + G_l \sin\varphi \\ g_z/2 \cos\psi &= G_l \cos\varphi \end{aligned} \tag{12}$$

where G_l is the magnitude of vector $\boldsymbol{G}_l$. Solving for ψ and g_z we obtain:

$$\psi = \arctan\left(\frac{g_0 + g_{lz}}{2g_{lr}}\right) \tag{13}$$

$$g_z = \frac{g_0 + g_{lz}}{\sin\psi} \tag{14}$$

Consequently, we can control the motion and the orientation of a microrobot in the three-dimensional space (x, y, z) using magnetic forces, by controlling the magnitude of the magnetic field gradient produced by the H_z coils, and the direction of the magnetic field, with the following expression:

$$\mathbf{B} = \begin{bmatrix} B\cos\psi\cos\theta & B\cos\psi\sin\theta & B\sin\psi \end{bmatrix} \tag{15}$$

where $\theta = \arctan(x/y)$, $\psi = \arctan(z/r)$, and $r = (x^2+y^2)^{1/2}$.

C. VERIFICATION OF THE PROPOSED SYSTEM

To demonstrate the proposed modified system, we modified a general Helmholtz coils system that was originally designed to work with one power supply per pair of coils. Fig. 4(a) and (b) show the lateral and front views of the electromagnetic system used in experiments, and its working space. The coil system is composed of three pairs of circular Helmholtz coils (whose parameters are summarized in Table 1) enclosed within water-cooled circular steel containers, allowing operation for large periods of time. We powered the H_{z1} and H_{z2} coils using two AC/DC sources (GW Instek, APS-1020) with a maximum RMS current of 10 A, while the remaining two pairs of coils were powered with two AC/DC power sources (GW Instek, GKP-2302) with a maximum RMS current of 30 A. The H_z coils generate the maximum magnetic field gradient that can be produced at maximum power, as can be observed in Table 1, explaining why we decided to control these two coils independently in our experiments; selecting any other pair of coils would

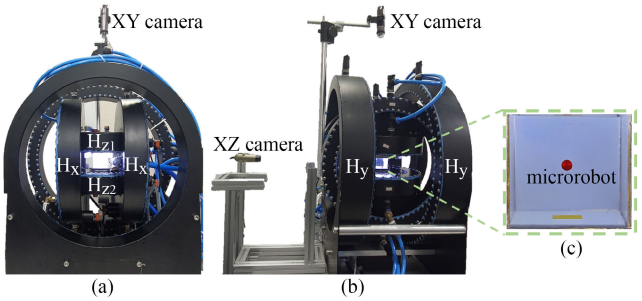

FIGURE 4. (a) Front view of the coil system showing the upper camera (XY plane), the H_x pair of coils, and coils H_{z1} and H_{z2}. (b) Side view of the coil system showing the H_y pair of coils, the upper camera, and the side camera (XZ plane). (c) Acrylic box filled with silicone oil containing the spherical magnetic microrobot.

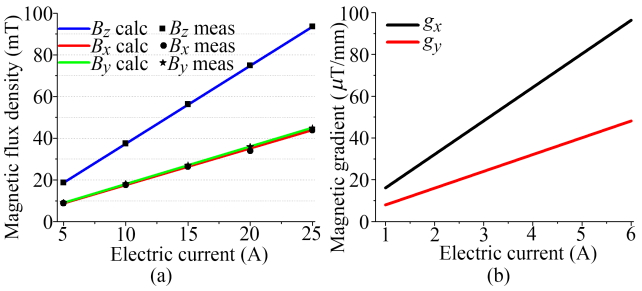

FIGURE 5. (a) Variation of magnetic flux density at the center of the H_x, H_y, and H_z pair of coils with electric current. Lines indicate calculated values, while points indicate measurements. (b) Calculated magnetic gradient field at the center of the H_z pair of coils for different values of electric current.

have achieved the same results with respect to combination of UMFs with a GMF. We tested two different magnetic microrobots in these experiments: a permanent magnet microrobot and a temporarily magnetized microrobot. The permanent magnet microrobot consists of a spherical N35 neodymium magnet with a diameter of 5 mm. This robot was painted red to facilitate image-processing-based tracking. The temporarily magnetized microrobot, a magnetic disk with a diameter and height of 1.5 mm, was fabricated using a 3D printer (FlashForce Guider II) and iron-filled polylactic acid (PLA). The magnetization curve of this robot, used to calculate the magnetic force, was measured using a vibrating sample magnetometer (Lake Shore 7404).

Experiments were conducted in an acrylic container with a working space of 56 mm × 56 mm × 56 mm filled with silicone oil with a dynamic viscosity of 970 mPa· s (Shin-Etsu, KF-96H-1,000cs). Microrobots were placed inside the acrylic as shown in Fig. 4(c).

Motion in the XY plane was tracked using a USB camera (Dino-Lite, AM73915MZTL) with a framerate of 60 FPS, while a USB camera (Dino-Lite, AM4113FVT) with a framerate of 30 FPS tracked motion in the XZ plane.

Although k_x, k_y, k_z, and k_c can be calculated with the parameters of the coil, for more precise control, we measured the magnetic field produced by the coils to determine these constants experimentally. Here, we used a gaussmeter

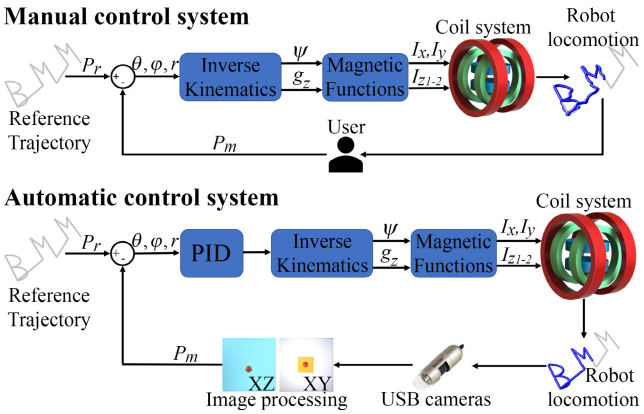

FIGURE 6. Block diagrams of the open and closed-loop control system.

(F.W. Bell 5180) to measure the uniform magnetic field produced by each pair of coils at the center of the system while varying the electric current from 5 A to 25 A in steps of 5 A, as shown in Fig. 5(a). Based on this, $k_x = 1.76$, $k_y = 1.8$ and $k_z = 3.74$. As the calculated and measured values of these constants were observed to be identical, we determined that calculated data is reliable for analysis of the gradient field. Fig. 5(b) shows the calculated values of g_z and g_r at the center of the coil for electric currents ranging from 1 A to 6 A. These values were used to determine that $k_g = 32$.

We developed a manual open-loop control (OLC) system and an automatic closed-loop control (CLC) system to direct the locomotion of the microrobots. The operation of these control systems is summarized in Fig. 6. With the manual OLC system, the user inputs a target trajectory for the microrobot as a set of points, $P_r = [x\ yz]$, that is subsequently displayed in the graphical user interface.

Then, the microrobot's direction of motion is set with two joysticks, which define the control angles θ and φ, and the desired r. The system uses these inputs to calculate the required orientation of the magnetic moment ψ and the value of g_z, using the inverse kinematics equations ((13) and (14)), following which, it obtains the requisite current for each pair of coils using the magnetic function equations ((2), (7), and (15)). The uniform magnetic field defines the orientation and direction of motion of the microrobot, while the gradient defines its speed. This control method requires constant manipulation from the user for the robot to completely traverse the input trajectory.

With the CLC system, the user introduces the required trajectory in cartesian coordinates. The program then converts this trajectory into spherical coordinates (θ, φ and r) and estimates the requisite current for each coil following the same steps as the OLC system. The two USB cameras measure the position of the robot (P_m) as it moves, and compares it with the reference position, to ensure travel is maintained on the input trajectory. The position of the robot is compensated by a PID controller, which parameters we tune

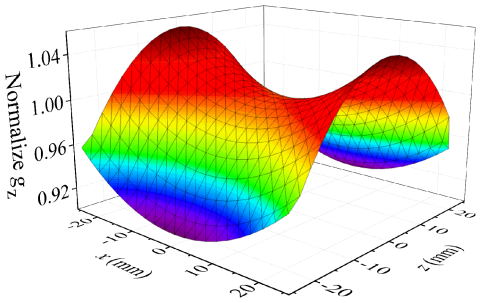

FIGURE 7. Normalized g_z at the XZ plane for y = 0, from calculations.

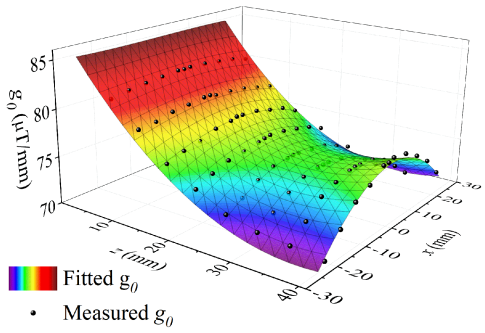

FIGURE 8. Measured (points) and fitted (contour) compensation magnetic gradient (g_0) at the ZX plane for y = 0.

using Ziegler–Nichols method for a quick test of the proposed system.

We analyzed the behavior of g_z in the ZR plane further, as shown in Fig. 7, finding that the value of g_z decreases as the robot moves either side of the z axis from the center, and increases as it moves away from the center to either side of the x axis. Consequently, I_{g0}, the current required to produce the compensation gradient (g_0) is not constant, as it varies as a function of the position of the robot. To ensure the CLC system could vary g_0 with position, we measured the value of g_0 at 25 different locations on the ZR plane, divided as a 5 point × 5 point mesh, and fitted this data to a prediction function that estimates the value of g_0 at any position of the ZR plane, as shown in Fig. 8.

As g_0 is inversely proportional to g_z, opposing trends are seen in both graphs. Because of the symmetry of the magnetic field, we can assume that the values of g_0 will be the same for any ZR plane. Hence, the generalization should be applicable for the entire 3D working space.

III. EXPERIMENTS AND RESULTS

To compare the performance of the gravity compensation algorithm with constant and varying g_0, we placed the permanent magnet robot in two different locations (P1 = [0 0 15] mm and P2 = [0 0 25] mm) and tracked its change in position, as seen in Fig. 9. Fig. 9(a) and (b) show that in the absence of a compensating magnetic force, the robot sinks, reaching the bottom of the container within 0.5 s from a starting position of P1, and 0.7 s from a starting position of P2. With g_0 defined as a constant,

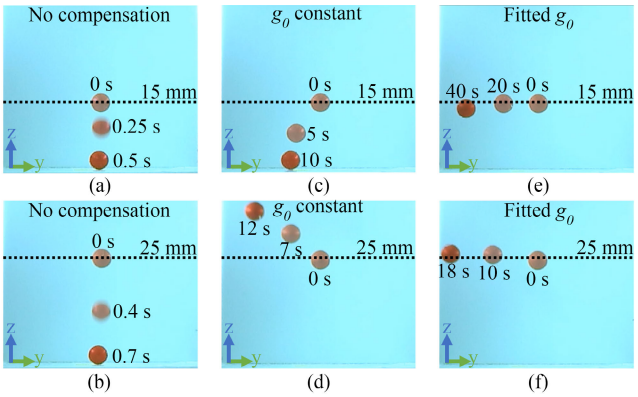

FIGURE 9. (a, b) Change in the position of the microrobot without gravity compensation, (c, d) with constant gravity compensation, and (e, f) with 2D fitted gravity compensation, with initial position z = 15 mm (a, c, e) and z = 25 mm (b, d, f).

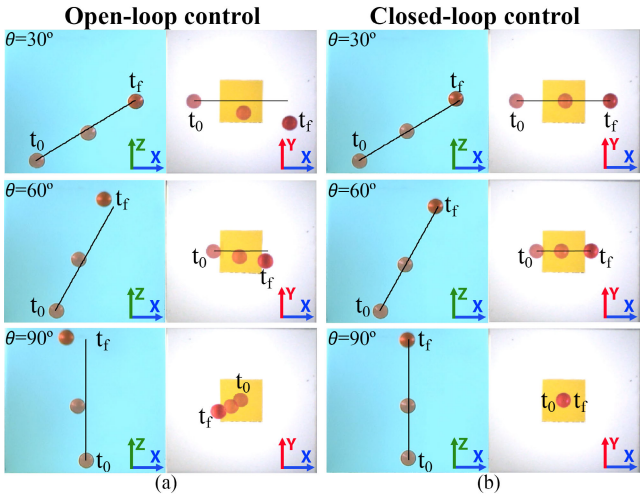

FIGURE 10. Timelapse images of the magnetic microrobot travelling at angles of 30°, 60°, and 90° with respect to the x-z axis, for open-loop control (a) closed-loop control (b).

the robot sank to the bottom of the container within 10 s when its initial position was P1, as shown in Fig. 9(c). Conversely, when its initial position was P2, the robot was slowly dragged upwards, disappearing from the working space after 12 s, as shown in Fig. 9(d). In contrast, with the fitted values of g_0, the vertical position of the magnet barely changed, as shown in Fig. 9(e) and (f). In all cases, there was a slow variation in the horizontal position of the robot, which was primarily caused by the small contribution of $\delta \mathbf{B}_r/\delta z$.

To analyze the efficiency of the proposed electromagnetic system in combination with the gravity compensation algorithm, we measured the position of the permanent magnet microrobot while moving it along straight lines with angles varied from 0° to 90° with respect to the x-z axis, in steps of 10°. We performed experiments five times each with the OLC (no camera feedback, nor position control) and CLC systems, with results as shown in Fig. 10.

Fig. 10 shows how the position of the robot changes as the robot moved along 30°, 60°, and 90° angles in the ZX plane with open-loop control (a), and closed-loop control (b). With

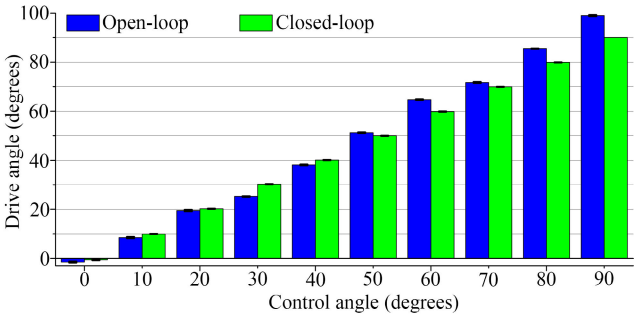

FIGURE 11. Comparison of control and drive angles for open and closed loop control systems.

the CLC, the robot followed the straight line at the given angle perfectly in both the ZX plane and the XY plane. In contrast, although the robot was able to follow the 30° line perfectly with the OLC, a slight offset from the 60° and 90° lines can be observed. Offsets were also generated in the XY plane with all the three cases. The actual drive angles of the microrobot are plotted with respect to the control angles for all straight lines tested in Fig. 11, for comparison of the OLC with the CLC. Variation between the drive angles was negligible for both OLC (below 0.32°) and CLC (below 0.16°), indicating high repeatability. With the CLC, the actual drive angle was practically the same as the control angle, with the largest mean error of 0.5° obtained when the control angle was 0°. However, with the OLC, the error changed significantly with each control angle, with drive angles of 25.2°, 64.7°, 85.5°, and 99.9° noted for control angles of 30°, 40°, 80°, and 90°, respectively.

Fig. 12 presents a comparison between the locomotion of the microrobot when using the developed manual open-loop control (OLC) system and that when using the automatic close-loop control (CLC) system (Movie S1). The microrobot was controlled along a 3D trajectory composed of the letters BMM, with each letter located at different coordinates Z (10 mm, 20 mm, and 30 mm). We repeated each experiment five times.

Fig. 12(a) and (b) show images of the microrobot while moving along the BMM trajectory under the OLC and CLC systems, respectively. Fig. 13(a) shows the measured position of the microrobot along the BMM trajectory when using the OLC system in the 3D space, whereas Fig. 13(b) shows the measured position under the OLC system.

To evaluate the accuracy of the control algorithm, we considered the robot to be in the desired position if the difference between the measured position and the control position was less than 0.8 mm. For the OLC system, a significant error was observed mainly in the z coordinate; this was primarily owing to the inability of the user to control both joysticks with sufficient precision. However, precision can be improved, albeit at the cost of locomotion speed. In general, the OLC had a mean error of 982.8 ± 87 μm, mean speed of 3.9 ± 0.05 mm/s, and mean accuracy of 57.3%. For the CLC system, the graphs indicate that the robot position perfectly matched the desired

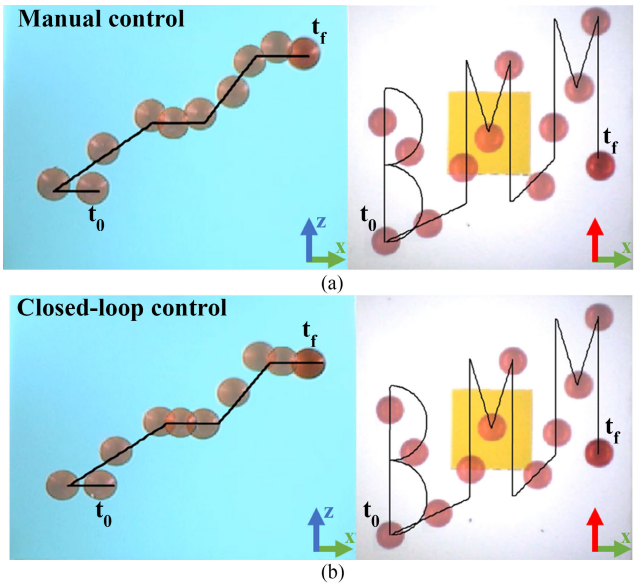

FIGURE 12. Timelapse images of the locomotion of the magnetic microrobot under (a) manual control and (b) automatic closed-loop control in a BMM trajectory.

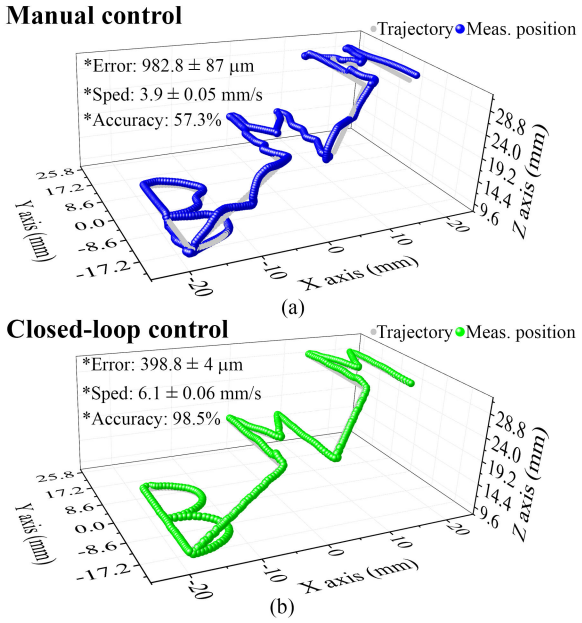

FIGURE 13. Graphs indicating the desired trajectory and measured position of the microrobot in a 3D space under (a) manual control and (b) automatic closed-loop control.

trajectory, with a mean error of 398 ± 4 μm, mean speed of 6.1 ± 0.06 mm/s, and mean accuracy of 98.5%.

To further evaluate the performance of the CLC in navigation, we tracked the permanent magnet robot as it followed two different 3D trajectories, as shown in Fig. 14, performing each experiment five times (Movie S2). Fig. 14(a) shows images captured of the microrobot as it followed a 3D trajectory composed of zigzags, sinusoids, straight lines, and loops.

Fig. 14(b)–(d) show the actual position of the microrobot at different points along the trajectory in the 3D space, and

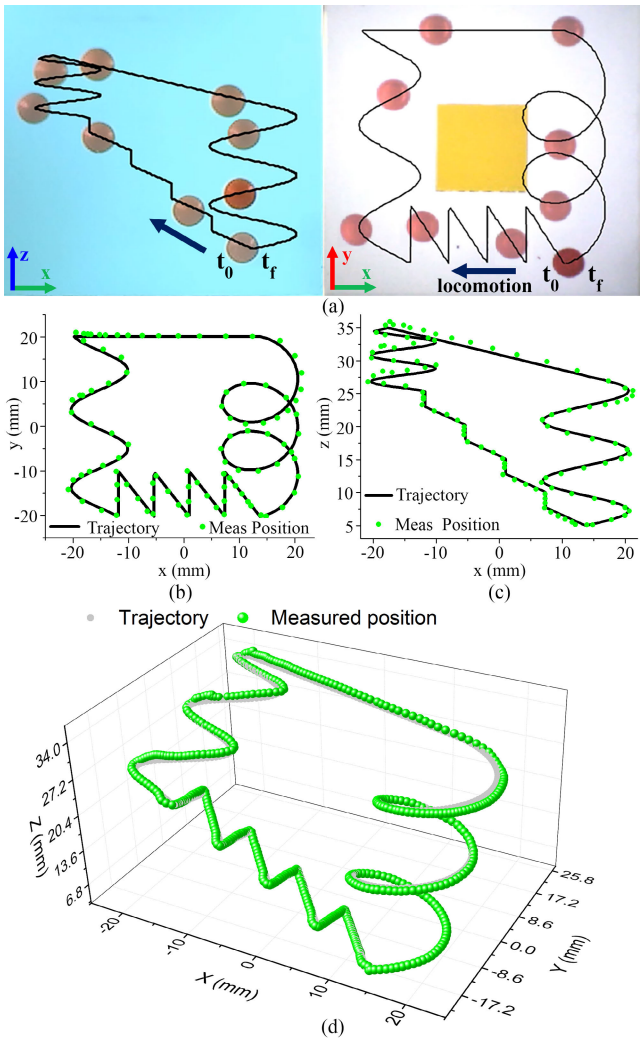

FIGURE 14. (a) Timelapse image of the magnetic microrobot traversing a 3D trajectory composed of straight lines, zigzags, sinusoids, and loops, automated by closed-loop control. Comparison of the desired trajectory with the measured position of the microrobot in the (b) XY plane, (c) ZX plane, and (d) three-dimensional space.

the XY and XZ planes. From this image, it can be observed that the measured position matches the input trajectory, with a mean error of 526 ± 8.2 μm and a mean accuracy of 96.2% obtained at a mean speed of 6.4 ± 0.18 mm/s.

We performed an additional experiment to demonstrate that the proposed system and control algorithm can be used for the actuation of temporarily magnetized microrobots, such as those including iron powder, or similar magnetic nanoparticles, in their composition, by directing the motion of a 3D-printed magnetic PLA disk on the surface of a heavy fluid (sodium metatungstate solution) (Movie S3). Fig. 15(a) shows images captured of the magnetic disk moving along a spiral trajectory. From Fig. 15(b), it can be observed that the measured position perfectly matches the reference trajectory (100% accuracy), with a mean error of 135 ± 2 μm (11× smaller than the diameter of the microrobot), obtained at a mean speed of 1.68 ± 0.05 mm/s.

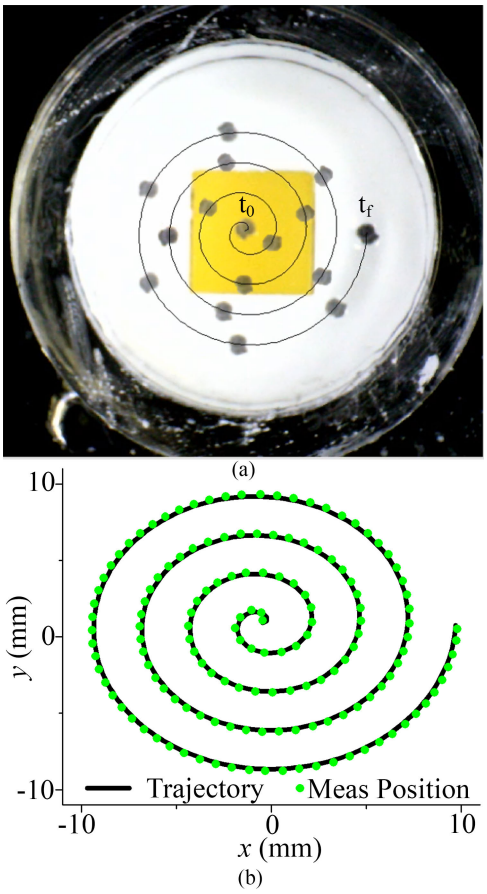

FIGURE 15. (a) Timelapse image of the magnetized disk robot following a spiral trajectory. (b) Graph comparing the spiral trajectory with the measured position of the disk robot.

IV. CONCLUSION

In this paper, we proposed the modification of a 3D Helmholtz coil system, to enable production of a gradient magnetic field, in addition to a uniform magnetic field, without investing a lot of money. The modification consists of splitting the pair of coils in one axis, such that each coil is controlled individually, while the remaining two pairs of coils are maintained in their original configuration. Because the modified axis can be selected arbitrarily and only one additional power supply is required, the proposed modification can be easily applied to any existing 3D Helmholtz coils system.

The advantage of 3D Helmholtz coil systems is their simplicity; since the only variables controlled are the three electric currents flowing through the magnetic coils, and because the magnetic field generated by these systems is uniform, these parameters do not depend on the position of the robot in the working space. We demonstrated that the simplicity of such systems can be maintained, by developing a control algorithm that also considers the gradient produced by the modified coils as a constant, adding only one more control variable to the overall system.

Our results show that the system can produce a 3D magnetic force with 1 DOF, while being able to control the magnetic force-based 3D locomotion of a spherical magnetic microrobot. The developed control algorithm works with acceptable precision in an open-loop situation, even when the influence of gravity is significant. Furthermore, when using closed-loop control, a gravity compensating gradient can be measured and fitted to a predictive function beforehand, to increase the precision of the system. With this process, precisions above 96% and mean errors below 400 μm, more than ten times smaller than the length of our microrobot, were achieved in all experiments, demonstrating the micrometric resolution possible with our algorithm.

In experiments conducted with the magnetic disk, the mean error decreased by a factor of five, as a result of positioning the camera closer to the controlled object. Similarly, we noted that the maximum speed attained by the permanent magnet microrobot was limited by the speed of the cameras. Hence, the demonstrated speed and precision of the control system can be improved simply by changing the cameras, with no further modification required to the control algorithm.

REFERENCES

[1] J. Hwang, J.-Y. Kim, and H. Choi, "A review of magnetic actuation systems and magnetically actuated guidewire- and catheter-based microrobots for vascular interventions," *Intell. Service Robot.*, vol. 13, no. 1, pp. 1–14, Jan. 2020.

[2] Z. Yang and L. Zhang, "Magnetic actuation systems for miniature robots: A review," *Adv. Intell. Syst.*, vol. 2, no. 9, Sep. 2020, Art. no. 2000082.

[3] S. H. Kim and K. Ishiyama, "Magnetic robot and manipulation for active-locomotion with targeted drug release," *IEEE/ASME Trans. Mechatronics*, vol. 19, no. 5, pp. 1651–1659, Oct. 2014.

[4] J. Guo, Z. Bao, Q. Fu, and S. Guo, "Design and implementation of a novel wireless modular capsule robotic system in pipe," *Med. Biol. Eng. Comput.*, vol. 58, no. 10, pp. 2305–2324, Oct. 2020.

[5] S. Jeon, G. Jang, H. Choi, and S. Park, "Magnetic navigation system with gradient and uniform saddle coils for the wireless manipulation of micro-robots in human blood vessels," *IEEE Trans. Magn.*, vol. 46, no. 6, pp. 1943–1946, Jun. 2010.

[6] H. Choi, K. Cha, J. Choi, S. Jeong, S. Jeon, G. Jang, J.-O. Park, and S. Park, "EMA system with gradient and uniform saddle coils for 3D locomotion of microrobot," *Sens. Actuators A, Phys.*, vol. 163, no. 1, pp. 410–417, Sep. 2010.

[7] Q. Fu, S. Guo, Q. Huang, H. Hirata, and H. Ishihara, "Development and evaluation of novel magnetic actuated microrobot with spiral motion using electromagnetic actuation system," *J. Med. Biol. Eng.*, vol. 36, no. 4, pp. 506–514, Aug. 2016.

[8] K. E. Peyer, S. Tottori, F. Qiu, L. Zhang, and B. J. Nelson, "Magnetic helical micromachines," *Chem. A, Eur. J.*, vol. 19, no. 1, pp. 28–38, Jan. 2013.

[9] D. Byun, J. Choi, K. Cha, J.-O. Park, and S. Park, "Swimming microrobot actuated by two pairs of Helmholtz coils system," *Mechatronics*, vol. 21, no. 1, pp. 357–364, Feb. 2011.

[10] Q. Fu, S. Zhang, S. Guo, and J. Guo, "Performance evaluation of a magnetically actuated capsule microrobotic system for medical applications," *Micromachines*, vol. 9, no. 12, Dec. 2018, Art. no. 641.

[11] G.-H. Jeon and S. H. Kim, "Development and verification of mechanism for enhancement of steering angle and active locomotion for magnetic micro active-guidewire," *IEEE Access*, vol. 8, pp. 31103–31113, 2020.

[12] W. Lee, J. Nam, J. Kim, E. Jung, and G. Jang, "Effective locomotion and precise unclogging motion of an untethered flexible-legged magnetic robot for vascular diseases," *IEEE Trans. Ind. Electron.*, vol. 65, no. 2, pp. 1388–1397, Feb. 2018.

[13] S. Jeong, H. Choi, K. Cha, J. Li, J.-O. Park, and S. Park, "Enhanced locomotive and drilling microrobot using precessional and gradient magnetic field," *Sens. Actuators A, Phys.*, vol. 171, no. 2, pp. 429–435, Nov. 2011.

[14] K. Choi, S. M. Jeon, J. K. Nam, and G. H. Jang, "A magnetic minirobot with anchoring and drilling ability in tubular environments actuated by external magnetic fields," *J. Appl. Phys.*, vol. 117, no. 17, May 2015, Art. no. 17A730.

[15] J. Nam, W. Lee, J. Kim, and G. Jang, "Magnetic helical robot for targeted drug-delivery in tubular environments," *IEEE/ASME Trans. Mechatron.*, vol. 22, no. 6, pp. 2461–2468, Dec. 2017.
[16] Y. H. Ha, B. H. Han, and S. Y. Lee, "Magnetic propulsion of a magnetic device using three square-Helmholtz coils and a square-Maxwell coil," *Med. Biol. Eng. Comput.*, vol. 48, no. 2, pp. 139–145, Feb. 2010.
[17] Q. Cao, X. Han, B. Zhang, and L. Li, "Analysis and optimal design of magnetic navigation system using Helmholtz and Maxwell coils," *IEEE Trans. Appl. Supercond.*, vol. 22, no. 3, Jun. 2012, Art. no. 4401504.
[18] J. K. Nam, S. M. Jeon, W. S. Lee, and G. H. Jang, "Control of a three-dimensional magnetic force generated from a magnetic navigation system to precisely manipulate the locomotion of a magnetic microrobot," *J. Appl. Phys.*, vol. 117, no. 17, May 2015, Art. no. 17A726.
[19] H. Choi, K. Cha, S. Jeong, J.-O. Park, and S. Park, "3-D locomotive and drilling microrobot using novel stationary EMA system," *IEEE/ASME Trans. Mechatronics*, vol. 18, no. 3, pp. 1221–1225, Jun. 2013.
[20] S. Song, S. Song, and M. Q.-H. Meng, "Electromagnetic actuation system using stationary six-pair coils for three-dimensional wireless locomotive microrobot," in *Proc. IEEE Int. Conf. Inf. Autom. (ICIA)*, Macau, China, Jul. 2017, pp. 305–310.
[21] Q. Zhang, S. Song, P. He, H. Li, H.-Y. Mi, W. Wei, Z. Li, X. Xiong, and Y. Li, "Motion control of magnetic microrobot using uniform magnetic field," *IEEE Access*, vol. 8, pp. 71083–71092, 2020.
[22] S. H. Kim, "3D Helmholtz coil-based hybrid manipulation for active locomotion of magnetic micro/nano robots," *J. Magn.*, vol. 23, no. 4, pp. 578–583, 2018.
[23] M. D. Tehrani, M. O. Kim, and J. Yoon, "A novel electromagnetic actuation system for magnetic nanoparticle guidance in blood vessels," *IEEE Trans. Magn.*, vol. 50, no. 7, Jul. 2014, Art. no. 5100412.
[24] J. Kim, M. J. Kim, J. Yoo, and S.-J. Kim, "Novel motion modes for 2-D locomotion of a microrobot," *IEEE Trans. Magn.*, vol. 50, no. 11, 2014, Art. no. 8500305.
[25] Q. Zhang, S. Song, and S. Song, "Study on magnetic field model of independent circular coils for wireless manipulation of microrobots," in *Proc. IEEE Int. Conf. Inf. Autom. (ICIA)*, Macau, China, Jul. 2017, pp. 1137–1142.
[26] G. Go, H. Choi, S. Jeong, C. Lee, S. Y. Ko, J.-O. Park, and S. Park, "Electromagnetic navigation system using simple coil structure (4 coils) for 3-D locomotive microrobot," *IEEE Trans. Magn.*, vol. 51, no. 4, Apr. 2015, Art. no. 8002107.
[27] K. T. Nguyen, M. C. Hoang, G. Go, B. Kang, E. Choi, J.-O. Park, and C.-S. Kim, "Regularization-based independent control of an external electromagnetic actuator to avoid singularity in the spatial manipulation of a microrobot," *Control Eng. Pract.*, vol. 97, Apr. 2020, Art. no. 104340.
[28] A. Chah, T. Kroubi, and K. Belharet, "A new electromagnetic actuation system with a highly accessible workspace for microrobot manipulation," in *Proc. IEEE/ASME Int. Conf. Adv. Intell. Mechtron. (AIM)*, Boston, MA, USA, Jul. 2020, pp. 723–728.
[29] S. Yuan, Y. Wan, and S. Song, "RectMag3D: A magnetic actuation system for steering milli/microrobots based on rectangular electromagnetic coils," *Appl. Sci.*, vol. 10, no. 8, Apr. 2020, Art. no. 2677.
[30] M. P. Kummer, J. J. Abbott, B. E. Kratochvil, R. Borer, A. Sengul, and B. J. Nelson, "OctoMag: An electromagnetic system for 5-DOF wireless micromanipulation," *IEEE Trans. Robot.*, vol. 26, no. 6, pp. 1006–1017, Dec. 2010.
[31] W. Lee, J. Nam, J. Kim, E. Jung, N. Kim, and G. Jang, "Steering, tunneling, and stent delivery of a multifunctional magnetic catheter robot to treat occlusive vascular disease," *IEEE Trans. Ind. Electron.*, vol. 68, no. 1, pp. 391–400, Jan. 2021.
[32] N. Kim, S. Lee, W. Lee, and G. Jang, "Development of a magnetic catheter with rotating multi-magnets to achieve unclogging motions with enhanced steering capability," *AIP Adv.*, vol. 8, no. 5, May 2018, Art. no. 056708.
[33] M. Hoang, V. Le, K. Nguyen, V. Nguyen, J. Kim, E. Choi, S. Bang, B. Kang, J.-O. Park, and C.-S. Kim, "A robotic biopsy endoscope with magnetic 5-DOF locomotion and a retractable biopsy punch," *Micromachines*, vol. 11, no. 1, p. 98, Jan. 2020.
[34] F. Munoz, G. Alici, and W. Li, "A magnetically actuated drug delivery system for robotic endoscopic capsules," *J. Med. Devices*, vol. 10, no. 1, pp. 1–13, Mar. 2016.
[35] J. Li, X. Li, T. Luo, R. Wang, C. Liu, S. Chen, D. Li, J. Yue, S.-H. Cheng, and D. Sun, "Development of a magnetic microrobot for carrying and delivering targeted cells," *Sci. Robot.*, vol. 3, no. 19, Jun. 2018, Art. no. eaat8829.
[36] D. Kim, H. Lee, S. Kwon, Y. J. Sung, W. K. Song, and S. Park, "Hydrogel microrobots: Bilayer hydrogel sheet-type intraocular microrobot for drug delivery and magnetic nanoparticles retrieval (Adv. Healthcare Mater. 13/2020)," *Adv. Healthcare Mater.*, vol. 9, no. 13, Jul. 2020, Art. no. 2070040.

ARMANDO RAMOS-SEBASTIAN (Graduate Student Member, IEEE) received the B.S. degree in bionics engineering from the Instituto Politecnico Nacional (IPN), Mexico City, Mexico, in 2016, and the M.S. degree in electronics convergence engineering from Wonkwang University, Iksan, South Korea, in 2020. He is currently pursuing the Ph.D. degree in convergence technology engineering with Jeonbuk National University, Jeollabuk-do, South Korea.

His current research interests include design and control of magnetic micro-robots for targeted drug delivery, magnetic hyperthermia, and magnetic particle imaging.

SUNG HOON KIM (Member, IEEE) received the B.S. degree in electronic engineering from Yeungnam University, Gyeongsan, South Korea, in 2005, the M.S. degree in medical and biological engineering from Kyungpook National University, Daegu, South Korea, in 2007, and the Ph.D. degree in electrical communication engineering from Tohoku University, Sendai, Japan, in 2012.

He is currently an Associate Professor with the Department of Electronic Convergence Engineering, Wonkwang University, Iksan, South Korea. His research interests include magnetic sensors and actuators, multi-scale magnetic micro/nano systems, magnetic hyperthermia, and implantable medical devices.